NJC

PAPER

View Article Online
View Journal | View Issue

Cite this: *New J. Chem.*, 2014, **38**, 5254

EPR based distance measurement in Cu-porphyrin–DNA†

ThaoNguyen Nguyen,‡[a] Pär Håkansson,[a] Ruth Edge,§[b] David Collison,[b] Bernard A. Goodman,[c] Jonathan R. Burns¶[a] and Eugen Stulz*[a]

Received (in Montpellier, France) 11th May 2014,
Accepted 18th August 2014

DOI: 10.1039/c4nj00673a

www.rsc.org/njc

EPR spectroscopy was used to investigate both single and double stranded DNA modified with a variable number of copper(II) porphyrins. The spectra of the porphyrin–DNA complexes resemble those of the Cu(II) porphyrin building blocks, but with appreciable differences in the values for the $g_{\|}$ and $A_{\|}$ parameters. In addition, a significant half-field signal is observed, which is interpreted as resulting from copper–copper interactions in both the double strand (dsDNA) and the single strand DNA (ssDNA). Analysis of the EPR spectra gives evidence for cluster formation of three or more DNA strands. From the intensity ratio of the half-field and main transition, the average Cu–Cu distance is estimated to be 6.5–8.9 Å. The association of copper centres is consistent with hydrophobic porphyrin stacking, both intra- and intermolecularly, as has previously been observed with other DNA complexes using UV-vis and CD spectroscopy.

1. Introduction

The use of DNA as a supramolecular scaffold for functional molecules has emerged as a powerful tool in bio-nanotechnology,[1,2] including the realization of smart nanomachines,[3–5] biomimetic materials,[6] DNA templated synthesis[7] and DNA origami.[8–10] In particular covalent modifications using a variety of substituents has led to systems which act as helical chromophore templates,[11–14] potential electronic devices[15] and sensors.[16,17] Attachment of substituents, however, may alter the structure and properties of DNA significantly, and the impact is still not fully understood. Aromatic and hydrophobic moieties such as pyrenes[18] or porphyrins[19] tend to show strong intra- and intermolecular interactions, directly impacting the behavior of modified DNA; this has been shown by UV-vis and CD spectroscopy, and by SAXS analysis[20] of multi-porphyrin assemblies. Here, we present new direct evidence of intermolecular interactions in modified DNA using EPR spectroscopy of copper metallated porphyrin–DNA.

EPR spectroscopy has been widely applied to the analysis of paramagnetic biomolecules, including derivatives of DNA. Investigations of DNA using EPR spectroscopy have mainly been performed using nitroxide spin labels.[21–23] In contrast, there are very few reports of EPR analyses of DNA–metal complexes: here the copper(II) was placed *inside* the base-pairing region of the DNA through chelating nucleobase analogues where a Cu–Cu distance of 3.7 ± 0.1 Å was estimated.[24–26] Cu(II) porphyrins have, on the other hand, been well studied, and have the potential to be excellent probes of the structure of DNA complexes. We have now analysed Cu(II) porphyrin oligo-deoxynucleotide (ODN) complexes in frozen matrix; by comparing their spectra with those of the free Cu(II) porphyrins insight is provided into the local structure and intermolecular interactions in porphyrin–DNA, presenting a complementary approach to existing methods. To our knowledge this is the first application of copper based EPR half-field transitions to estimate intra- and intermolecular distances in bio-molecules.

In our design, the porphyrin is held in a rigid position and thus can be very sensitive to the local structural environment of the DNA. We have also developed an efficient protocol for specific Cu(II) metallation on the DNA.[20] Two different porphyrin structures were chosen for this analysis, namely diphenyl and tetraphenyl porphyrin (DPP and TPP, Fig. 1), which produce DNA complexes with different properties: DPP tends to be more hydrophobic and shows stronger excitonic coupling between adjacent units compared to TPP.[27] It should be noted that control experiments did not reveal any residual copper ions present in solution or otherwise bound to DNA.

[a] *School of Chemistry and Instituted of Life Sciences, University of Southampton, Highfield, Southampton, SO17 1BJ, UK. E-mail: est@soton.ac.uk*
[b] *School of Chemistry and Photon Science Institute, The University of Manchester, Oxford Road, Manchester, M13 9PL, UK*
[c] *State Key Laboratory for Conservation and Utilization of Subtropical Agro-Bioresources, Guangxi University, Nanning 530005, Guangxi, China*

† Electronic supplementary information (ESI) available: Full EPR spectroscopic analyses are given. See DOI: 10.1039/c4nj00673a

‡ Present address: Reckitt Benckiser Products Ltd, Dansom Lane, Hull HU8 7DS, UK.
§ Present address: Dalton Cumbrian Facility, The University of Manchester, Westlakes Science & Technology Park, Moor Row, Cumbria CA24 3HA, UK.
¶ Present address: Chemistry Department, University College London, 20 Gordon Street, London WC1H 0AJ, UK.

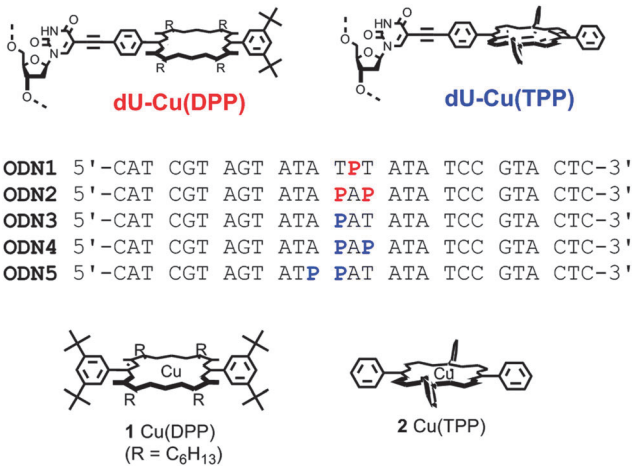

Fig. 1 Structures of the copper complexes of diphenyl porphyrin (DPP) and tetraphenyl porphyrin (TPP), and their attachment site in modified DNA strands.

2. Experimental

2.1. General procedure for copper metallation of porphyrin–DNA

The porphyrin–DNA was synthesised as published previously.[27,28] $Cu(OAc)_2{\cdot}H_2O$ (12.5 μL or 25 μL, 16 mM, 400 nmol, 200 eq.) was added to the porphyrin–DNA (100 μL, 10 μM, 1 or 2 nmol porphyrin equivalent) and immediately deoxygenated by purging with N_2 for 10 seconds, then stirred vigorously on a thermomixer at 85 °C for 5 min. The reaction mixture was then left to cool to room temperature for 5 min. EDTA pH 8.0 (100 μL, 400 mM, 40 μmol, 20 000 eq.) was added to quench excess $Cu(OAc)_2$, followed by buffer (100 μL, 100 mM NaCl, 50 mM KH_2PO_4, pH 7.0). 6 batches of this reaction were performed simultaneously, combined, followed by addition of water (200 μL) and the reaction mixture was purified *via* Glen-Pak cartridge to give copper metallated DNA (averaged 93%) as a dark purple solid. **ODN1**: UV-vis (H_2O, $c = 5 \times 10^{-6}$ M): $\lambda_{max}(\log \varepsilon)$ 261 (5.28), 410 (4.17) nm; emission (H_2O, $c = 5 \times 10^{-6}$ M): λ_{ex} 410 nm, λ_{em} (rel int) 632 (1), 693 (0.96) nm. **ODN2**: UV-vis (H_2O, $c = 5 \times 10^{-6}$ M): $\lambda_{max}(\log \varepsilon)$ 265 (5.38), 409 (5.37) nm; emission (H_2O, $c = 5 \times 10^{-6}$ M): λ_{ex} 409 nm, λ_{em} (rel int) 637 (1), 695 (0.75) nm. **ODN3**: UV-vis (H_2O, $c = 5 \times 10^{-6}$ M): $\lambda_{max}(\log \varepsilon)$ 260 (5.46), 422 (4.81) nm; emission (H_2O, $c = 5 \times 10^{-6}$ M): λ_{ex} 422 nm, λ_{em} (rel int) 651 (1), 713 (0.32) nm. **ODN4**: UV-vis (H_2O, $c = 5 \times 10^{-6}$ M): $\lambda_{max}(\log \varepsilon)$ 264 (5.46), 423 (5.14) nm; emission (H_2O, $c = 5 \times 10^{-6}$ M): λ_{ex} 423 nm, λ_{em} (rel int) 656 (1), 713 (0.35) nm. **ODN5**: UV-vis (H_2O, $c = 5 \times 10^{-6}$ M): $\lambda_{max}(\log \varepsilon)$ 260 (5.49), 423 (5.28) nm; emission (H_2O, $c = 5 \times 10^{-6}$ M): λ_{ex} 423 nm, λ_{em} (rel int) 654 (1), 716 (0.28) nm.

2.2. EPR spectroscopy, general

All samples of copper porphyrin building blocks were investigated under three separate conditions: pure solid powder, fluid solution and frozen solution. Cu-porphyrin–DNA complexes were only measured as frozen solutions at 120 K, because of limited sample availability for pure solid measurements and the high molecular mass which produced rigid limit spectra from fluid solutions. For porphyrin building blocks DCM, and DCM : toluene 9 : 1 were used as solvents for fluid and frozen solution spectra, respectively, and Cu-porphyrin–DNA complexes were investigated in DNA grade water. The EPR spectra were acquired using Bruker EMX-X band (approx. 9 GHz) and Bruker EMX Micro-X band (approx. 9 GHz). Low temperature spectra were acquired with variable temperature cryostats using liquid nitrogen as coolant for measurements in the temperature range 120–301 K. All samples were measured in quartz tubes with internal diameters of 3 mm (X-band). Spectra were acquired with 100 kHz modulation frequency in the field range 0–8000 (X-band) Gauss using the Bruker WIN-EPR program. Initial peak positions were estimated using WIN-EPR and these were then used to provide a basic interpretation of the spectra; all hyperfine coupling constants (A_{iso}, $A_{\parallel}$, $A_{\perp}$) are quoted in Gauss. Concentrations of 100, 200 and 300 μM were explored, with the case of 300 μM shown in the figures.

2.3. Parameter estimation for copper porphyrin building blocks

The frozen solution EPR experiment (120 K) is analysed with the solid state line shape function (pepper) in EasySpin.[29] The pepper function allows for a computed powder average using second order perturbation theory for ^{14}N ligands and matrix diagonalization for electronic energy levels. The spin Hamiltonian in pepper includes electronic Zeeman, the $^{63}Cu(II)$ and $^{65}Cu(II)$ isotropic nuclear Zeeman (weighted at natural abundance ratio), Cu(II) hyperfine and four ^{14}N superhyperfine interactions. The routine pepper provides line broadening to mimic a frozen solution spectrum. Isotropic broadening of Gaussian form is used. Anisotropic parameters have a cylindrical symmetry as is expected for a square planar complex. In this work the inhomogeneous broadening of the so-called H-strain, g-strain are used. Minimization of eqn (1) was done:

$$\chi^2 = \frac{1}{N}\sum_{i=1}^{N}\frac{\left(I'(B_i)_{EXP} - I'(B_i)_{SIM}\right)^2}{\sigma^2}, \qquad (1)$$

where $I'(B_i)_{YYY}$ YYY = [EXP,SIM] are experimental and simulated first derivative spectra, $N = 1500$ is the number of experimental points representing the whole spectrum, σ^2 is the experimental variance estimated from the tail of spectra. Minimization of χ^2 was done with the Matlab function fminsearch (using the Nelder–Mead simplex algorithm). For best fit parameters see Table S1 (ESI†).

Note that there are several routes for which parameter estimation in Table S1 (ESI†) can be done, both at the level of approximation in the numerical line shape calculation as well as in the number and type of phenomenological broadening parameters (here σR, $\sigma H_{\perp}$ and $\sigma H_{\parallel}$ are used). However, the above procedure was found in a recent study[30] to give the set of spin-Hamiltonian parameters for porphyrin **1** that also consistently explains the lineshapes in fluid solution 197–293 K. Note first, the liquid state study was performed with rigorous non-perturbative simulation techniques. Secondly, both porphyrins were prepared by identical procedures, thus providing confidence

in both parameter sets in Table S1 (ESI†). The agreement with the liquid state study also indicates that no significant freezing artefact was introduced upon freezing the sample.[31]

We provide qualitative simulation of fluid solution spectra in Fig. S2 and S3 (ESI†) and computed with the expression $a + bm_I + cm_I^2$ for the linewidths (L/W) of the copper peaks.[32] The lack of quantitative predictive power comes from a slow molecular tumbling on EPR time scale. A detailed study of fluid solution copper porphyrin is performed elsewhere.[30]

2.4. Cu–Cu distance calculation in the porphyrin–DNA

The spectra are baseline corrected with a first order polynomial ($ax + b$). 1st-derivative spectrum (Fig. S5, ESI†) is integrated to provide the absorption spectra in Fig. S6 (ESI†); see also Fig. 3. Finally the absorption spectra are integrated to provide area($|\Delta M_s| = 2$) and area($|\Delta M_s| = 1$) with:

$$I_{rel} = \text{area}(|\Delta M_s| = 2)/\text{area}(|\Delta M_s| = 1) = K_0/r^6 \qquad (2)$$

The distance, r, between the paramagnetic centres[33] is given from I_{rel} in eqn (2) with $K_0 = 21$ (Å^6).

3. Results and discussion

In order to understand the basic EPR properties of the copper metallated porphyrin–DNA strands (Fig. 1), we have compared them with the individual porphyrins **Cu(TPP) 1** and **Cu(DPP) 2**. The syntheses of **1** and **2** were reported previously.[30,34]

3.1. Analysis of the porphyrins Cu(DPP) and Cu(TPP)

The powder spectra (Fig. S1, ESI†) of the porphyrins **1** and **2** produced broad single peaks because of electron dipolar interactions between neighbouring paramagnetic sites, but resolution of parallel and perpendicular components was seen with frozen solutions (Fig. 2). The EPR spectrum of **2** has previously been reported.[34] An extensive EPR study of porphyrin **1** in frozen as well as a wide range of fluid solution temperatures was performed by some of us.[30] Spin-Hamiltonian parameters were first determined from frozen solution. Then the validity of the parameters was verified with fluid solution EPR experiments analyzed with a rigorous non-perturbation simulation.[30] Hence, the study provides confidence in the challenging parameter estimation from frozen solution EPR experiments. Furthermore, the sample preparation followed in this work can be expected not to contain freezing artefacts.[31] A slow fluid state overall molecular tumbling with fast local porphyrin dynamics was determined.[30] Simulations of spectra (Fig. 2) with g and A matrices assuming square planar Cu coordination (axial symmetry) gave similar parameters for both complexes (Table 1), indicating that there is little difference in the electronic structure of the metal centers of **1** and **2**. These results are consistent with the unpaired electron density being located primarily in the $d_{x^2-y^2}$ orbital, despite symmetry differences for the complexes (C_{2v} in **1**, D_{4h} in **2**). Super-hyperfine structure (shfs) from ^{14}N indicates that the molecular orbital contains appreciable ligand contributions.[31] Overall, the EPR measurements are comparable to other data

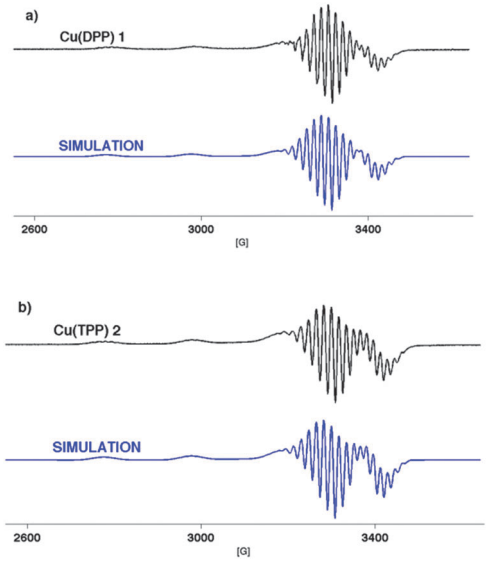

Fig. 2 Frozen solution EPR spectra (1st derivative) of **Cu(DPP) 1** (a) and **Cu(TPP) 2** (b) at 120 K and simulated spectra in upper and lower trace respectively; simulation parameters are in Table 1 and the lineshape information in ESI.†

Table 1 EPR parameters obtained by simulation of the frozen solution (120 K) spectra of Cu(II) porphyrins **1** and **2** based on the natural abundance weighted ^{63}Cu, ^{65}Cu isotopes, hyperfine parameters in Gauss (see ESI for details)

Porphyrin	g_{iso}	A_{iso} (^{63}Cu)	A_{iso} (^{14}N)	$g_\perp$	$g_\parallel$	$A_\perp$ (^{63}Cu)	$A_\parallel$ (^{63}Cu)	$A_\perp$ (^{14}N)	$A_\parallel$ (^{14}N)
Cu(DPP) 1	2.094	84.4	16.0	2.045	2.191	20.6	211.9	17.1	13.8
Cu(TPP) 2	2.094	84.1	16.0	2.046	2.189	20.9	210.5	16.8	14.5

reported in the literature for Cu(II) porphyrin complexes.[34–36] No signals were observed in the range of 1200–2500 G (see Fig. S4, ESI†). This suggests there is no close intermolecular interaction of the individual Cu(II) building blocks in the organic solvent.

3.2. EPR spectra of Cu(porphyrin)–DNA

The spectra of the copper metallated ODN strands were recorded in the frozen state (120 K, water as solvent). The ODNs were measured either as single or as a double strand, where the appropriate complementary strand contains no Cu(II) porphyrin. The measurements show similar fingerprints in the main region of the EPR spectra at $g \sim 2$; Fig. 3 shows the spectra of **ODN3** in single and double stranded form as a representative example (see ESI† for all spectra). An exception is **dsODN1** that did not produce an EPR spectrum of acceptable quality even in the frozen matrix; thus this sample was excluded from the analysis. Interestingly, all of the copper porphyrin–DNA strands produced a secondary feature around 1600 G ($g \approx 4.3$).

The ODN EPR results are understood by considering a system consisting of two electron spins (*i.e.* two Cu-porphyrins). The main electron-spin transition (~3300 G) is the allowed triplet state transition ($|\Delta M_s| = 1$) and the half-field is the "forbidden"

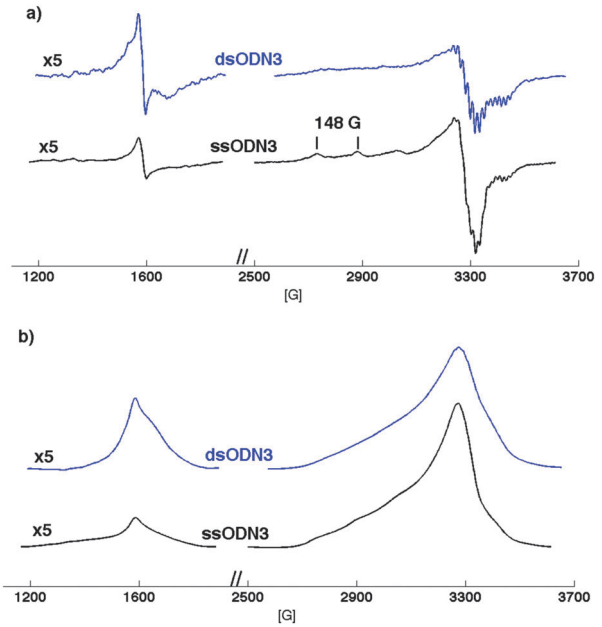

Fig. 3 (a) Frozen solution EPR spectra (1st derivative) of **ssODN3** (black) and **dsODN3** (blue) at 120 K; (b) absorption spectra for **ODN3** obtained from integration of the 1st derivative spectra, left panel shows the half field transition (magnified 5-times).

transition ($|\Delta M_s| = 2$). Since no half-field transition was observed with the control Cu porphyrin samples, the half-field signal is an intrinsic property of the copper porphyrin–DNA system. In addition, control experiments rule out iron impurities which could also give rise to a signal at $g = 4.3$.[37] Clearly, for the single porphyrin strands a direct Cu–Cu interaction can only occur through intermolecular interactions.

3.3. Distance evaluation in the porphyrin–DNA

Perturbation theory applied to the spin Hamiltonian dictates that the half-field transition is allowed provided that there are anisotropic interactions.[38] Dipole–dipole (DD) interactions thus increase the amount of anisotropic interaction as the Cu–Cu distance shortens and/or with increasing number of interactions. Under the assumption that the DD interaction is the dominant anisotropic interaction (compared to anisotropic spin–spin coupling), the half-field transition provides a convenient means to estimate Cu–Cu distances. A particularly simple approach would be to assume *only* a pairwise interaction and estimate distances from $I_{rel} = K_0/r^6$, where K_0 is a proportionality constant and $I_{rel} = I(|\Delta M_s| = 2)/I(|\Delta M_1| = 1)$,[38,39] a formula with expected validity for $r > 4$ Å.[35] This approach gives distances in the range of 4–5 Å for all samples (see Section 5, ESI†). However, such a short distance corresponds to a DD interaction of around 190 G and should significantly affect the main transition with a visible splitting that we cannot observe in the spectra (Fig. 3). A line shape fit of the main transition of the spectra (see Section 6, ESI†) shows that indeed the DD interaction predicted from $I(|\Delta M_1|)$ is much smaller and cannot be larger than 66 G. In addition, the modelled I_{rel} is two orders of magnitudes too small. We conclude that this inconsistency means a failure of the pair wise interaction model in our system. In order to better match the data we derive a multiple ODN pair model (Section 7, ESI†) using

$$I_{rel} = K_0\left(\frac{N}{r_{eff}^3}\right)^2, \quad (3)$$

where $K_0 = 21$ Å^6, N is the total number of electron spin interactions and r_{eff} is the effective average Cu(II)–Cu(II) distance in a cluster of ODNs. It should be noted that DD interactions give a larger weight to short distances, *i.e.* r_{eff} is not an arithmetic mean value.

The essential aspect of the model in eqn (3) is that it provides a route to explain the large half field intensity in terms of multiple weak interactions. In this way the model does not provide an inconsistent main field transition with a large DD splitting. In brief, 2–8 ODNs are considered to form clusters of copper centres. Depending on the sequence of the ODN this corresponds to one or two Cu(II) per ODN. The distances are calculated by first integrating the 1st-derivative spectra, and secondly integration of the absorption spectra (Fig. 3), providing the intensity ratios (I_{rel}) and distances for three, four or six ODNs listed in Table 2 (see Table S3 for all data, ESI†).

Qualitatively, the spectra at different concentrations all show similar relative intensity (100, 200 and 300 μM, data not shown). We choose to limit the quantitative interpretation to experiments that allow a base line correction with linear polynomial. In Table 2 the distances from 300 μM and illustrative cases of 100 μM concentrations are included, showing that the distances are approximately constant. The constant intensity ratio with concentration suggests that there is no significant amount of monomer in this concentration interval. In the following discussion we focus on the 300 μM samples since these have a better signal to noise ratio for analysis.

Without further assumption of a detailed geometrical model, it is clear from the data (Table S3, ESI†) that 1 pair for all ODNs

Table 2 Relative half-field intensity and computed distance for Cu(II)porphyrin–DNA as single strand (ss) and double stranded (ds) systems from experimental frozen solution spectra. Effective distance (r_{eff}) is given for a six ODN cluster of **ODN1** and **ODN3**, a four ODN cluster of **ODN2** and a three ODN cluster of **ODN4** and **ODN5**. For colour coding of base sequences see Fig. 1

Compound	Conc. (μM)	Local base-sequence	I_{rel}	r_{eff} (Å)
ssODN1	300	A TPT A	0.024	7.6(8)
ssODN1	100		0.024	7.6(3)
ssODN2	300	A PAP A	0.032	8.9(6)
dsODN2	300		0.064	7.9(8)
ssODN3	300	A PAT A	0.030	7.3(9)
dsODN3	300		0.056	6.6(5)
dsODN3	100		0.063	6.5(0)
ssODN4	300	A PAP A	0.017	8.0(8)
dsODN4	300		0.031	7.3(3)
dsODN4	100		0.04	6.9(9)
ssODN5	300	TP PAT	0.019	7.9(7)
dsODN5	300		0.048	6.8(2)

as well as the case of 3–4 ODNs for **ssODN1**, **ssODN3** and **dsODN3** can be ruled out as candidates. This is because of insufficient DD interaction to explain the half field intensity. Considering that higher order clusters may become too crowded to be reasonable models we select and present in Table 2 the three, four or six ODN models.

The values for r_{eff} indicate that the copper centres have a minimal distance of around 6.5–8.9 Å. The distances correspond well to the centre-to-centre distances which can be found in π-stacked porphyrins in XRD structures (around 8 Å),[40] and also to what would be expected from porphyrins being attached to DNA in adjacent positions (9.7 Å)[27] as in **ODN5**. The rather large range of distances indicates that the intra- and intermolecular interactions strongly depend on the ODN system.

From a model point of view, the porphyrins are far enough outside the DNA groove to allow stacking with other DNA strands (Fig. 4). The DNA strands do not need to approach close enough to induce a steric clash. Since the helicity of the double helix prevents perfect stacking of four porphyrins on two different duplexes, the fourth porphyrin would instead be twisted away from the stack, and is available to interact with a third porphyrin–DNA strand, leading to the three- or four-DNA bundles. Previous SAXS measurement clearly showed formation of discrete assemblies,[20] for which this model would provide a suitable picture. However, without direct structural data, *e.g.* from XRD or NMR structure determination, this model remains hypothetical.

3.4. EPR parameters of Cu(porphyrin)–DNA

In Table 3 a selection of EPR parameters is given, determined by a direct measurement from the spectra (see ESI†). Although the $g_\perp$ and $A_\perp(^{14}N)$ values are comparable to those for the corresponding copper porphyrin building blocks for all porphyrin–DNA strands, there is a significant decrease by ~60 G in the $A_\parallel$(Cu) values, an increase by ~0.09 in the $g_\parallel$ values and by ~0.04 in g_{iso}. The low field shift (increased g_{iso}-value) is actually expected in the presence of Cu(II) interactions.[38,41] In principle the resonance shift could provide an additional route to estimate the Cu(II)–Cu(II) distance, although this is a less sensitive method, and was not considered here. The origins of these shifts are not entirely clear at this stage; though a reduced $A_\parallel$(Cu) may be explained with a deviation in square planar coordination, this will give constant or reduced $g_\parallel$ as well[42] and is thus not a likely explanation. However, the changes are in line with those reported for copper uroporphyrin III dimers in aqueous solutions.[41]

Table 3 EPR parameters for Cu(II)porphyrin–DNA as single strand (ss) and double stranded (ds) systems from experimental frozen solution spectra

Compound	$g_\perp$	$g_\parallel$	$A_\parallel$ (^{63}Cu)/G	$A_\perp$ (^{14}N)/G
ssODN1	2.04	2.29	148	nd
ssODN2	2.05	2.29	150	17
dsODN2	2.05	2.27	150	17
ssODN3	2.05	2.28	148	17
dsODN3	2.05	2.30	148	17
ssODN4	2.05	2.28	150	17
dsODN4	2.05	2.30	150	17
ssODN5	2.05	2.27	150	17
dsODN5	2.04	2.30	150	17

We also note that spectra of the ODNs recorded in fluid solution at room temperature have a signal that is too broad to allow detailed analysis. Such extreme broadening can be expected in the presence of dipole–dipole interaction *combined* with a slowly tumbling complex. Hence, since a direct Cu–Cu interaction can be observed, the experiment suggests that the porphyrin–DNA is also associated at room temperature.

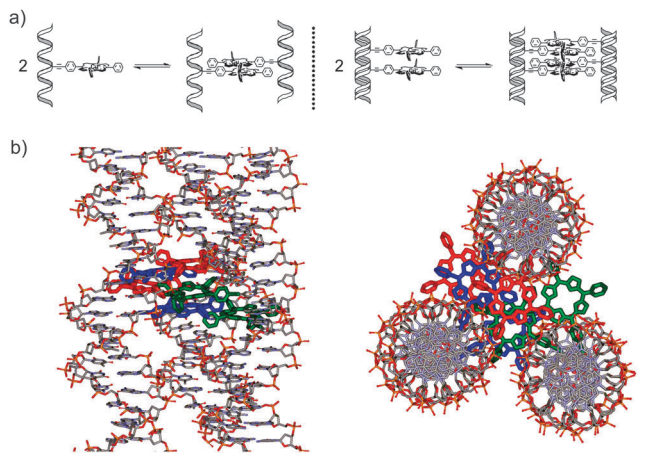

Fig. 4 (a) Schematic representation of the self-association of porphyrin–DNA strands in single and double stranded form for **ssODN3** and **dsODN4**; (b) proposed model of a trimer formed by **dsODN4** as side-view and top-view.

4. Conclusions

In summary, we present the first EPR spectroscopic analysis of copper(II) centres covalently attached to the outer rim of DNA through porphyrins as ligands; the spectra compare well to the spectra reported for CuN_4 complexes formed on G-quadruplexes.[43] A semi-quantitative model of cluster formation of Cu-porphyrin bearing ODNs is formulated. The model allows for average Cu distances within the clusters to be estimated from EPR data, and a minimum cluster size to be established. Effective distances are consistent with discrete clustering of several porphyrin–DNA with π-stacking of the porphyrins, supporting previous reports of intermolecular interactions between centres. Therefore the attachment of large hydrophobic substituents to DNA leads to additional interactions that need to be taken into account when designing functional molecules based on a DNA scaffold. These interactions, on the other hand, can be exploited as molecular glues between DNA strands, adding an orthogonal tool to the design in DNA bio-nanotechnology.

Acknowledgements

This work was supported through the EPSRC PhD-PLUS scheme (Fellowship to TNN). The EPSRC MS Centre Swansea and the EPSRC UK National Electron Paramagnetic Resonance Service

at The University of Manchester are greatly acknowledged for their services.

Notes and references

1 E. Stulz, *Chem. – Eur. J.*, 2012, **18**, 4456–4469.
2 E. Stulz, G. Clever, M. Shionoya and C. Mao, *Chem. Soc. Rev.*, 2011, **40**, 5633–5635.
3 Y. Krishnan and F. C. Simmel, *Angew. Chem., Int. Ed.*, 2011, **50**, 3124–3156.
4 C. Song, Z. G. Wang and B. Q. Ding, *Small*, 2013, **9**, 2382–2392.
5 M. von Delius and D. A. Leigh, *Chem. Soc. Rev.*, 2011, **40**, 3656–3676.
6 J. M. Galloway, J. P. Bramble and S. S. Staniland, *Chem. – Eur. J.*, 2013, **19**, 8710–8725.
7 M. L. McKee, P. J. Milnes, J. Bath, E. Stulz, R. K. O'Reilly and A. J. Turberfield, *J. Am. Chem. Soc.*, 2012, **134**, 1446–1449.
8 R. Schreiber, J. Do, E. M. Roller, T. Zhang, V. J. Schuller, P. C. Nickels, J. Feldmann and T. Liedl, *Nat. Nanotechnol.*, 2014, **9**, 74–78.
9 J. Yoo and A. Aksimentiev, *Proc. Natl. Acad. Sci. U. S. A.*, 2013, **110**, 20099–20104.
10 J. R. Burns, K. Gopfrich, J. W. Wood, V. V. Thacker, E. Stulz, U. F. Keyser and S. Howorka, *Angew. Chem., Int. Ed.*, 2013, **52**, 12069–12072.
11 T. Nguyen, A. Brewer and E. Stulz, *Angew. Chem., Int. Ed.*, 2009, **48**, 1974–1977.
12 D. Baumstark and H. A. Wagenknecht, *Chem. – Eur. J.*, 2008, **14**, 6640–6645.
13 M. Probst, S. M. Langenegger and R. Häner, *Chem. Commun.*, 2014, **50**, 159–161.
14 P. Roethlisberger, F. Wojciechowski and C. J. Leumann, *Chem. – Eur. J.*, 2013, **19**, 11518–11521.
15 K. Borjesson, J. Tumpane, T. Ljungdahl, L. M. Wilhelmsson, B. Norden, T. Brown, J. Martensson and B. Albinsson, *J. Am. Chem. Soc.*, 2009, **131**, 2831–2839.
16 S. P. Sau and P. J. Hrdlicka, *J. Org. Chem.*, 2012, **77**, 5–16.
17 I. Grabowska, D. G. Singleton, A. Stachyra, A. Gora-Sochacka, A. Sirko, W. Zagorski-Ostoja, H. Radecka, E. Stulz and J. Radecki, *Chem. Commun.*, 2014, **50**, 4196–4199.
18 D. Baumstark and H. A. Wagenknecht, *Angew. Chem., Int. Ed.*, 2008, **47**, 2612–2614.
19 A. Mammana, G. Pescitelli, T. Asakawa, S. Jockusch, A. G. Petrovic, R. R. Monaco, R. Purrello, N. J. Turro, K. Nakanishi, G. A. Ellestad, M. Balaz and N. Berova, *Chem. – Eur. J.*, 2009, **15**, 11853–11866.
20 A. Brewer, G. Siligardi, C. Neylon and E. Stulz, *Org. Biomol. Chem.*, 2011, **9**, 777–782.
21 U. Jakobsen, S. A. Shelke, S. Vogel and S. T. Sigurdsson, *J. Am. Chem. Soc.*, 2010, **132**, 10424–10428.
22 O. Schiemann, N. Piton, Y. Mu, G. Stock, J. W. Engels and T. F. Prisner, *J. Am. Chem. Soc.*, 2004, **126**, 5722–5729.
23 P. Z. Qin and T. Dieckmann, *Curr. Opin. Struct. Biol.*, 2004, **14**, 350–359.
24 K. Tanaka, G. H. Clever, Y. Takezawa, Y. Yamada, C. Kaul, M. Shionoya and T. Carell, *Nat. Nanotechnol.*, 2006, **1**, 190–194.
25 K. Tanaka, A. Tengeiji, T. Kato, N. Toyama and M. Shionoya, *Science*, 2003, **299**, 1212–1213.
26 G. H. Clever, S. J. Reitmeier, T. Carell and O. Schiemann, *Angew. Chem., Int. Ed.*, 2010, **49**, 4927–4929.
27 I. Bouamaied, T. Nguyen, T. Rühl and E. Stulz, *Org. Biomol. Chem.*, 2008, **6**, 3888–3891.
28 L. A. Fendt, I. Bouamaied, S. Thöni, N. Amiot and E. Stulz, *J. Am. Chem. Soc.*, 2007, **129**, 15319–15329.
29 S. Stoll and A. Schweiger, *J. Magn. Reson.*, 2006, **178**, 42–55.
30 P. Håkansson, T. Nguyen, P. B. Nair, R. Edge and E. Stulz, *Phys. Chem. Chem. Phys.*, 2013, **15**, 10930–10941.
31 J. S. Hyde and W. Froncisz, *Annu. Rev. Biophys. Bioeng.*, 1982, **11**, 391–417.
32 R. C. Sealy, J. S. Hyde, C. C. Felix, I. A. Menon, G. Prota, H. M. Swartz, S. Persad and H. F. Haberman, *Proc. Natl. Acad. Sci. U. S. A.*, 1982, **79**, 2885–2889.
33 J. Svorec, M. Valko, J. Moncol, M. Mazur, M. Melnik and J. Telser, *Transition Met. Chem.*, 2009, **34**, 129–134.
34 K. L. Cunningham, K. M. McNett, R. A. Pierce, K. A. Davis, H. H. Harris, D. M. Falck and D. R. McMillin, *Inorg. Chem.*, 1997, **36**, 608–613.
35 B. A. Goodman and M. V. Cheshire, *Nat. New Biol.*, 1973, **244**, 158–159.
36 B. A. Goodman and M. V. Cheshire, *Eur. J. Soil Sci.*, 1976, **27**, 337–347.
37 T. Suzuki, Y. Maeda, H. Sakai, S. Fujimoto and Y. Morita, *J. Biochem.*, 1975, **78**, 555–560.
38 A. Bencini and D. Gatteschi, *Electron Paramagnetic Resonance of Exchange Coupled Systems*, Springer-Verlag GmbH, New York, 1990.
39 S. Eaton and G. Eaton, in *Distance Measurements in Biological Systems by EPR*, ed. L. Berliner, G. Eaton and S. Eaton, Springer, US, 2002, pp. 1–27.
40 E. Stulz, S. M. Scott, Y. F. Ng, A. D. Bond, S. J. Teat, S. L. Darling, N. Feeder and J. K. M. Sanders, *Inorg. Chem.*, 2003, **42**, 6564–6574.
41 W. E. Blumberg and J. Peisach, *J. Biol. Chem.*, 1965, **240**, 870–876.
42 J. Peisach and W. E. Blumberg, *Arch. Biochem. Biophys.*, 1974, **165**, 691–708.
43 D. M. Engelhard, R. Pievo and G. H. Clever, *Angew. Chem., Int. Ed.*, 2013, **52**, 12843–12847.